Published in final edited form as:
Clin Cancer Res. 2013 June 1; 19(11): 2850–2860. doi:10.1158/1078-0432.CCR-12-3084.

Translation initiation factor eIF3b expression in human cancer and its role in tumor growth and lung colonization

Hong Wang[1,2], **Yuanbin Ru**[1,2], **Marta Sanchez-Carbayo**[3], **Xuejiao Wang**[4,^], **Jeffrey S. Kieft**[5], and **Dan Theodorescu**[1,2,6,*]

[1]Department of Surgery (Urology), University of Colorado, Aurora, CO

[2]Department of Pharmacology, University of Colorado, Aurora, CO

[3]Spanish National Cancer Institute (CNIO), Madrid, Spain

[4]Department of Molecular Physiology, University of Virginia, Charlottesville, VA

[5]Howard Hughes Medical Institute and Department of Biochemistry and Molecular Genetics, University of Colorado, Aurora, CO

[6]University of Colorado Comprehensive Cancer Center, Aurora, CO

Abstract

Purpose—Discovery transcriptomic analyses suggest eukaryotic initiation factor 3b (eIF3b) is elevated in human bladder and prostate cancer, yet its role as a prognostic factor or its requirement in the maintenance or progression of human cancer is not established. Here we determine the therapeutic potential of eIF3b by examining the clinical relevance of its expression in human cancer tissues and its role in experimental tumor models.

Experimental Design—We examined mRNA expression of eIF3b in bladder (N=317) and prostate (N=566) tissue samples and protein expression by immunohistochemistry in 143 bladder tumor samples as a function of clinicopathologic features. The impact of eIF3b depletion by siRNA in human cancer lines was evaluated in regards to *in vitro* cell growth, cell cycle, migration, *in vivo* subcutaneous tumor growth and lung colonization.

Results—eIF3b mRNA expression correlated to tumor grade, stage and survival in human bladder and prostate cancer. eIF3b protein expression stratified survival in human bladder cancer. eIF3b depletion reduced *in vitro* cancer cell growth; inhibited G1/S cell cycle transition by changing protein but not RNA expression of Cyclin A, E, Rb and p27Kip1; inhibited migration and disrupted actin cytoskeleton and focal adhesions. These changes were associated with decreased protein expression of integrin α5. Integrin α5 depletion phenocopied effects observed with eIF3b. eIF3b depleted bladder cancer cells formed fewer subcutaneous tumors that grew more slowly and had reduced lung colonization.

Conclusion—eIF3b expression relates to human bladder and prostate cancer prognosis, is required for tumor growth and thus a candidate therapeutic target.

Keywords

eIF3b; cell cycle; integrin α5; tumor growth; tumor metastasis

*Corresponding author: Dan Theodorescu, University of Colorado Comprehensive Cancer Center, Aurora, CO 80045, Phone: (303)724-7135, FAX: (303)724-3162, dan.theodorescu@ucdenver.edu.
^Current Address: Cellomics Technology, LLC, Rockville, MD

INTRODUCTION

Deregulated protein synthesis and degradation contribute to cancer genesis and progression. Control of protein synthesis directs both global and selective translation of specific mRNAs, the protein products then promote tumor cell survival, angiogenesis, invasion and metastasis (1). Protein synthesis in eukaryotes is primarily regulated at initiation, the rate-limiting step and one that involves a large number of eukaryotic initiation factors (eIFs). To date, well over a dozen eIFs have been identified, several operating within large multi-protein complexes (2, 3). The components of several of these complexes are aberrantly expressed or activated in different types of human cancer (1, 4). Hence, targeting such factors offers promise for the development of a new class of cancer therapeutics. For example, overexpression of eIF4E is associated with poor prognosis in several human cancers (5) yet despite this factor being previously considered rate limiting in cap-dependent protein synthesis, its depletion with siRNA did not cause host toxicity in mice (6). This led to clinical trials in cancer patients using eIF4E siRNA (6–8).

Recent transcriptomic analyses carried out in the context of biomarker discovery (9–11) suggested that eukaryotic initiation factor 3b (eIF3b) may be elevated in human bladder and prostate cancer. eIF3b is a subunit of the eIF3 translation initiation factor complex. This complex has a molecular weight of 550–700 kDa and consists of 13 putative subunits in humans (12). By virtue of increased expression of several of its subunits (13) the eIF3 complex has been implicated in cancer. For example, eIF3a (p170) is overexpressed in several human cancers (13) and its depletion by antisense cDNA reversed the malignant phenotype in human cancer cells (14). Overexpression of a truncated eIF3e mutant caused transformation of mammary epithelial cells both *in vitro* and *in vivo* (15). eIF3h, located on chromosome region 8q, is frequently amplified in breast, prostate cancer and non-small cell lung cancer alone with the adjacent MYC pro-oncogene and its overexpression promotes cancer cell growth (16, 17). The eIF3b (hPrt1) subunit is particularly interesting since it serves a critical scaffolding function for the entire eIF3 complex (12, 18, 19). Indeed, ectopic overexpression of eIF3b transforms NIH3T3 cells (20), and overexpression of this protein is observed in breast cancer (21). However, these data fall short of implicating eIF3b as a prognostic factor or requirement for the maintenance or progression of human cancer.

Here we show that eIF3b is overexpressed in human bladder and prostate cancer and higher expression is associated with advanced grade, stage and poor prognosis. Using complementary molecular approaches in multiple cellular models *in vitro* and *in vivo*, we demonstrate that eIF3b expression is important to the malignant phenotype and consequently, as with eIF4E, eIF3b may be a viable therapeutic target in cancer.

MATERIALS AND METHODS

Bladder cancer microarray datasets and analysis for eIF3b mRNA expression

Two publicly available microarray datasets were used for the analysis of eIF3b expression in bladder cancer. The preprocessed data of "Kim *et al.*" (22) was downloaded from Gene Expression Omnibus (GEO, http://www.ncbi.nlm.nih.gov/geo/, accession GSE13507). The raw data of "Stransky *et al.*" (23) was downloaded from ArrayExpress (http://www.ebi.ac.uk/arrayexpress/, accession E-TABM-147) and normalized using the Robust Multichip Average algorithm (24). Patient demographics and clinicopathologic data is shown in Supplementary Table S1.

If there are multiple probe sets for eIF3b in a dataset, the probe set with the highest mean expression across samples was selected to represent eIF3b expression. The two datasets were mean centered so that samples have mean expression of zero in each dataset. Dotplots

of eIF3b expression comparing different groups of samples were plotted and differences in distributions were tested by Mann-Whitney U tests. To check whether eIF3b expression stratifies disease specific patient survival, patients were divided into two groups using the 70^{th} percentile of eIF3b expression and compared using Cox proportional hazards models and log rank tests.

Bladder cancer tissue microarray and immunohistochemistry

Bladder cancer tissue microarrays (TMAs) were constructed at the Spanish National Cancer Center (details in the Supplementary Materials and Methods), including a total of 143 bladder tumors (70 non-muscle invasive T1G3 and 73 muscle invasive T2–4 tumors). Protein expression patterns of eIF3b were assessed using standard avidin–biotin immunoperoxidase procedures (25). The primary antibody for immunohistochemistry was eIF3b (LifeSpan Biosciences LS-C138931), rabbit monoclonal at 1:50. The secondary antibody was a biotinylated horse anti-rabbit antibody (Vector Laboratories, 1:1000 dilution).

eIF3b expression was evaluated as continuous variables based on the number of cells expressing the protein in the cytoplasm. The intensity of the staining was categorized from negative (−) to low (+), intermediate (++), and high (+++). The associations of these proteins with disease-specific overall survival were also evaluated using the log-rank test in those cases for which follow-up information were available. Disease-specific overall survival time was defined as the months elapsed between transurethral resection or cystectomy and death as a result of disease (or the last follow-up date). Patients who were alive at the last follow-up or lost to followup were censored. Survival curves were plotted using the standard Kaplan-Meier methodology (25). Statistical analyses were performed using the SPSS statistical package (version 18.0).

Cell culture, transfection and western blotting

UMUC3, Lul2 human bladder cancer cells were cultured in MEM plus 10% FBS, 1 mM Sodium Pyruvate. siRNA transfection was carried out using Oligofectamine (Invitrogen) according to the manufacturer's instructions. Pre-designed siRNA duplexes were purchased from Dharmacon as follows: eIF3b-3: 5'-GAGTATGAACGGTGCCTTATT-3'; eIF3b-4: 5'-AGAGATCAGTACAGTGTGATT-3'; Luciferase GL2: 5'-GTACGCGGAATACTTCGA-3'. Integrin α5 siRNA, a pool of 3 target-specific siRNAs, was purchased from Santa Cruz. For Western blot, transfected the cells were harvested after 72 hours and equal amounts of total proteins were subjected to SDS-PAGE and analyzed using specific antibody. Antibodies used for Western blot are listed in the Supplementary Materials and Methods.

Real-time reverse transcription-polymerase chain reaction analysis

Quantitative RT-PCR was carried out on iCycler Optical Module (Bio-Rad) with IQ SYBR Green fluorescent dye (Bio-Rad) included in the PCR to determine the amount of mRNA level. Total RNA was purified from cells using RNeasy Mini kit (Qiagen). Human 12p primers developed by our laboratory was used for tumor quantization in the lungs (26). DNA from mice lungs was purified using MasterPure™ DNA Purification Kit (Epicentre Biotech).

In vitro cell growth, migration and cell cycle analysis

Monolayer growth was evaluated by alamarBlue assay and anchorage independence growth by soft agar assay (27). Cell cycle was evaluated by propidium iodide (PI) staining as

described (27). Cell migration assay was carried out by Boyden Chamber assay as described (28).

Immunofluorescence analysis

Cells were plated on cover slips and transfected with eIF3b or GL2 control siRNA the day after. 72 hours later, cells were fixed with 4% formaldehyde and stained with phalloidin-AlexaFluo 594 (Molecular Probes) or anti-myosinIIA (Abcam) to visualize actin filaments. Anti-P-FAK (Invitrogen) or Paxillin (BD transduction) staining was used to identify focal adhesions and DAPI as a nuclear marker. Zeiss LSM 510-UX or Olympus FV1000 Laser Scanning confocal microscope was used for capturing immunofluorescence images.

Nascent Protein Synthesis

New protein synthesis was measured using Click-iT® Metabolic Labeling Reagents (L-azidohomoalanine), and the Click-iT protein reaction buffer kit from Invitrogen according to the manufacturer's instructions. Newly synthesized proteins were detected by anti-TAMRA antibody as per manufacturer's instructions (Thermo Scientific). Total protein loading on the gel is detected by ponceau S staining.

Subcutaneous tumor growth and lung colonization in mice

Female 6-week athymic mice (Ncr *nu/nu*) were obtained from the NCI. 24 hours after siRNA transfection, 10^6 of UMUC3 cells were injected subcutaneously, tumors were measured by calipers weekly and volume was calculated (29). For lung colonization, mice were injected via tail vein with 10^6 of Lul2 cells transfected with siRNA 24 hours later. The images of lung metastases were evaluated by Xenogen Bioluminescent imaging system (Caliper Life Sciences) as described (30) and quantified using IGOR Pro 4.09A image analysis software. Quantification of tumor in the lungs was performed by RT-PCR using human 12p primers as described (26).

RESULTS

High eIF3b expression is associated with aggressive phenotypes and poor outcome in human bladder cancer

Discovery transcriptomic analysis of human cancers using previously published and newly profiled tumor and cell line microarray data (9–11) noted that probes associated with eIF3b were increased in bladder and prostate cancer. To evaluate the clinical relevance of this finding we compared eIF3b expression in normal bladder urothelium versus tumors, low-grade versus high-grade, and Non-Muscle Invasive (NMI, pTa and pT1) versus Muscle Invasive (MI, pT2 and above) samples. We observed eIF3b mRNA expression was higher in cancer than normal in high-grade than low-grade samples (Supplementary Fig. S1A–B) and in MI than NMI samples (Fig. 1A). Higher eIF3b expression was also associated with worse patient outcome (Fig. 1B).

Next, we developed immunohistochemical (IHC) staining for formalin fixed paraffin embedded (FFPE) materials and carried it out on human bladder tumor samples. Western blot and staining of eIF3b overexpressing cell lysates or FFPE cell pellets showed specificity of the eIF3b antibody used for IHC (Supplementary Fig. S2A–B). Representative immunohistochemical results on human tumors are shown in Fig. 1C. The next set of analyses searched for associations with clinicopathologic variables of patients with bladder cancer. It was observed that both the number of tumor cells displaying cytoplasmic expression and the intensity of the cytoplasmic expression of eIF3b were significantly associated with tumor stage (Kruskall-Wallis, p=0.004, and p=0.036 respectively). Furthermore, tumors expressing cytoplasmic eIF3b in at least 80% of the cancer cells were

significantly associated with poor disease-specific survival (Fig. 1D). These observations indicated that increased cytoplasmic eIF3b is associated with higher tumor stage and shorter survival, consistent with the transcriptomic analysis. We also did a similar analysis on prostate cancer and found eIF3b mRNA expression was higher in prostate cancer compared to normal prostate tissue and had a positive correlation with Gleason score. Higher eIF3b expression was also associated with androgen independence and worse disease specific survival in prostate cancer patients (Supplementary Fig. S3A–D).

Depletion of eIF3b inhibits cancer cell growth by inhibition of G1/S transition

To determine the importance of eIF3b expression for cancer cell growth, we depleted eIF3b protein via transfer of siRNAs into human bladder (UMUC3, Lul2) and prostate (PC3, DU145) cancer cells. A time-course of eIF3b protein levels showed significant reduction at 48–96h post-transfection that lasted for 6 days (Supplementary Fig. S4). eIF3b depletion significantly reduced the proliferation of UMUC3 and Lul2 cells (Fig. 2A), findings that were recapitulated with PC3 and DU145 cells (Supplementary Fig. S5). We next evaluated the ability of eIF3b-depleted cancer cells to form colonies in soft agar. Compared to the control siRNA transfected cells, UMUC3 and Lul2 cells with reduced eIF3b had much lower numbers of colonies (Fig. 2B).

To begin identifying the mechanisms underlying these effects, we evaluated whether eIF3b depletion had any effect on the cell cycle. At 96 hours after transfection the percentage of cells in S phase was lower in samples treated with eIF3b siRNAs, with a concomitant increase in the G1 phase in both UMUC3 (Fig. 2C) and Lul2 cells (Supplementary Fig. S6A), compared to samples treated with non-relevant GL2 siRNA. Since this suggested inhibition of the G1/S transition, we sought to determine if any of the regulators involved in this process are affected by eIF3b depletion. Interestingly, Cyclin A, Cyclin E, Rb protein expression and Rb phosphorylation were significantly decreased with eIF3b knockdown in UMUC3 cells (Fig. 2D). Knockdown of eIF3b also led to an increase in cyclin-dependent kinase inhibitor p27Kip1 in UMUC3, Lul2 and PC3 cells (Fig. 2D, Supplementary Fig. S6B). In contrast, the protein levels of RhoGDP dissociation inhibitor 1 and 2, known suppressors of tumor growth (RhoGDI1) and colonization (RhoGDI2) in human bladder cancer (31–33) were not changed (Fig. 2D). Importantly, while cells transfected with eIF3b siRNA showed significantly decreased eIF3b mRNA, control GUSB and mRNA levels of the above mentioned genes were not altered by eIF3b depletion (Supplementary Fig. S6C). This data suggests that changes of protein levels of cell cycle regulators seen with depletion of eIF3b are not due to the changes of mRNA transcription and also that this effect is not general to all proteins.

Since eIF3b depletion led to reduced cell numbers *in vitro* (Fig. 2A), we sought to determine if apoptosis played a role in this process. We did not observe dramatic changes by Annexin V-FITC/PI staining apoptosis assay in response to eIF3b depletion (Supplementary Fig. S7A). Furthermore, we also analyzed the cell lysates by Western blotting, and did not observe cleaved PARP or activated Caspases (Supplementary Fig. S7B). These results indicate that no apoptosis was induced by eIF3b depletion.

Depletion of eIF3b decreases cancer cell migration, disrupts actin cytoskeleton organization and focal adhesion formation, and reduces integrin α5 expression

Cell migration is an important component of metastasis (34). Furthermore, the ability of cancer cells to attach successfully via focal adhesions to the extracellular matrix has been shown to be critical to both migration and growth at metastatic sites (35, 36). UMUC3 cells with eIF3b knockdown showed approximately 50% reduced transwell cell migration compared to control cells (Fig. 3A). We also observed dramatic cell morphology changes

after eIF3b depletion in UMUC3 and PC3, with eIF3b-depleted cells being smaller and rounded, suggesting impaired spreading compared with control cells (Fig. 3B; Supplementary Fig. S8A). Next we evaluated the intracellular distribution of proteins related to cell migration by immunofluorescence microscopy of UMUC3 cells. In control cells stained with phalloidin and myosin IIA for actin cytoskeleton evaluation, actin was present at the plasma membrane and formed stress fibers. In contrast, cells depleted of eIF3b revealed disorganization of the actin cytoskeleton, reduction of stress fibers and an increase of cortical actin (Fig. 3C). Similarly, we observed decreased vinculin (actin binding protein) staining in eIF3b-depleted PC3 cell (Supplementary Fig. S8A). Paxillin is an established marker of focal adhesions. Reduction of eIF3b levels led to a loss of paxillin distribution suggesting loss of focal adhesions in these cells (Fig. 3C). FAK, an important signaling molecule in the integrin pathway, localizes to and is activated (by autophosphorylation at Y397 site) within focal adhesions (37, 38). Consistent with the notion that eIF3b depletion induces focal adhesion disruption, this also led to decrease the phosphorylation of FAK in the focal adhesion (Fig. 3C). This was confirmed by Western blot with anti-phospho-FAK antibody (Fig. 3D). In contrast, overall levels of these proteins appeared unaltered by eIF3b depletion (Fig. 3D; Supplementary Fig. S8B). These results suggest that depletion of eIF3b decreases human bladder cancer cell migration in part by interrupting actin cytoskeleton organization and focal adhesion formation. Since FAK mediates several cell survival pathways we evaluated phosphorylation of Akt and found this was reduced in parallel to depletion of eIF3b and reduction of FAK phosphorylation (Fig. 3D).

Since integrins are upstream regulators of FAK, we sought to evaluate their expression as a function of eIF3b depletion. Western blot analysis revealed that integrin α5 protein level was dramatically decreased upon eIF3b knockdown in both UMUC3 and PC3 cells (Fig. 4A; Supplementary Fig. S8B), while other integrin proteins were not changed. Quantitation of integrin mRNA levels showed no statistically significant changes (Fig. 4B). Furthermore, we knocked down integrin α5 by siRNA in UMUC3 cells and observed that the cells were smaller and rounded, and had decreased spreading compared with control cells treated with GL2 siRNA (Fig. 4C), a phenocopy of the knockdown of eIF3b. Knockdown of integrin α5 also showed decreased phosphorylation of FAK and Akt, while the total protein levels stayed the same (Fig. 4D), similar to the effect observed upon knockdown of eIF3b Taken together, these data suggest the decreased cell migration and the change of cell morphology and adhesion induced by eIF3b knockdown is mediated in part through integrin α5.

Depletion of eIF3b decreases new protein synthesis

Given that depletion of eIF3b leads to many cell changes we wondered if this is caused by the decreasing of global protein synthesis or/and specific pool of proteins. To evaluate global protein synthesis we used the Click-iT metabolic labeling assay. As shown in Fig. 5A, untreated UMUC3 cells exhibited high levels of newly synthesized proteins, but as expected, protein synthesis was almost completely blocked by cycloheximide treatment. Reduction of eIF3b inhibited global protein synthesis by about 50% (Fig. 5A). Despite this, we found that upon eIF3b depletion, the total levels of some proteins were maintained compared to the untreated control while others decreased. Specifically, actin, GAPDH and FAK levels remain high, but the level of integrin α5 is decreased dramatically (Fig. 5B) in the samples with eIF3b depletion (Fig. 5C). This is consistent with the results of the total lysate Western blot (Fig. 3D and 4D; Supplementary Fig. S8B) and suggests that although global protein synthesis is inhibited by depletion of eIF3b, the effect on total protein levels may be specific to individual proteins.

To determine if the effect on global translation is eIF3b specific or more likely due to disruption of the eIF3 complex, we examined the expression levels of all thirteen eIF3 subunit mRNAs in human bladder cancer. In addition to eIF3b, both eIF3c and eIF3i were

higher in cancer than in normal in both data sets (Supplementary Table S3). We chose eIF3c to deplete based on the global architecture of eIF3, which places eIF3c at the center of the complex (12) and thus its depletion is more likely to affect the entire complex. In addition, eIF3c is increased in testicular seminomas (39) and ectopic overexpression of eIF3c transforms NIH3T3 (20) both findings supporting a role for this protein in cancer. Depletion of eIF3c significantly inhibited UMUC3 cell growth and new protein synthesis (Supplementary Fig. S9A and 9C), decreased integrin α5 expression, and disrupted actin cytoskeleton organization and focal adhesion formation (Supplementary Fig. S9B and S9D). Thus, changes induced by eIF3c depletion match those observed with eIF3b depletion, suggesting that the observed effects of depletion of either protein is due to an overall disruption of eIF3 complex stoichiometry or abundance which leads to the inhibition of translation.

Depletion of eIF3b decreases subcutaneous tumor growth and lung colonization

To determine the *in vivo* role of eIF3b expression in cancer, we injected UMUC3 cells transfected with control or eIF3b siRNA subcutaneously into mice and evaluated the kinetics of tumor formation and the growth of established tumors. eIF3b-depleted cells had delayed tumor formation and overall reduced tumor take (Fig. 6A). The tumors that did form grew more slowly compared to the group injected with control siRNA (Fig. 6B). We then investigated whether eIF3b was critical for bladder tumor colonization of the lung. To study this we selected Lul2 cells, a highly metastatic human bladder cell line (40). eIF3b-depleted Lul2 cells were inoculated in the tail vein of mice and bioluminescent *in vivo* imaging of metastases was carried out weekly. By five weeks after injection, imaging showed much stronger signals in GL2 siRNA group than those in eIF3b siRNA group (Fig. 6C). To confirm that these lung signals were indeed Lul2 cells, all mice were necropsied at five weeks and the tumor burden was quantified by qPCR with human specific primers on 12p (26). Compared to the GL2 siRNA group, the mice injected with Lul2 cells transfected with eIF3b siRNA showed dramatically less human genomic DNA (Fig. 6D). Importantly, the results of the tumor burden quantitated by qPCR were consistent with the quantitation of the radiance of luciferase (Fig. 6D) suggesting the latter was a true marker of lung colonization by human cancer cells.

DISCUSSION

While overexpression of eIF3b in mouse fibroblast cells causes transformation (20), until our work here, the role of eIF3b in human cancer was unclear. Data presented support a model in which eIF3b is required for maintenance of the malignant state. Knockdown of eIF3b inhibits cancer cells growth by inhibition of the G1/S cell cycle transition, but this did not seem to induce apoptosis of these cells. We investigated the molecular mechanism involved in cell cycle regulation by eIF3b. Given that eIF3b knockdown inhibits global translation and cyclins are unstable proteins (Supplementary Table S4) actively degraded in G1 phase, a reduction in protein synthesis would be expected to lead to reduced cyclin levels. This is consistent with our data (Fig. 2D). The observed increase in p27Kip levels along with decreased cyclins would also be expected to lead to hypophosphorylated Rb, which leads to G1 arrest (41). Also, G1 arrest is the major size regulatory "R or restriction point" checkpoint; if cells are too small they cannot pass this checkpoint (42). Since reduction in protein synthesis leads to smaller cells (Fig. 4C) we expected and indeed observed, eIF3b knockdown-induced translation depression to lead to arrest in G1 as a result of this checkpoint consistent with recent findings (43, 44).

In addition to the cell cycle effects, we found that lowering eIF3b levels in UMUC3 cells inhibited cell migration. We also observed cell morphology changes and decreased spreading. Cytoskeleton organization and adhesion formation are critical for cell motility

and structural support (45); our data indicates that eIF3b knockdown disrupts both, raising the question of how eIF3b regulates these processes. Integrins link the extracellular matrix (ECM) to intracellular cytoskeleton and focal adhesions and thus control a variety of signal transduction pathways including cell proliferation, survival (46). Depletion of eIF3b markedly inhibited integrin α5 expression, so integrin α5 might be one of eIF3b targets responsible for the disrupted actin cytoskeleton and focal adhesion. This is supported by our observation that knockdown of integrin α5 phenocopied the morphological changes seen with depletion of eIF3b. Knockdown of eIF3b and integrin α5 also had similar effects on the phosphorylation of FAK and Akt, which is significant since Akt plays a key role in cell proliferation and survival. This suggests that dramatically decreased bladder cancer cell growth induced by the depletion of eIF3b is not only due to effects on the cell cycle but also by effects on integrin/FAK/Akt signaling that are induced by a decrease in protein synthesis. Finally, since integrin α5 promotes cancer cell invasion and metastasis formation (47–49), our data supports the idea that the decreased integrin α5 induced by the knockdown of eIF3b contributes to the inhibition of lung colonization in bladder cancer.

Consistent with its role in translation initiation, depletion of eIF3b inhibited global protein synthesis (Fig. 5A), but interestingly not all protein levels were decreased equally (Fig. 2–4D and 5B), probably because not all mRNAs had an equal decrease in translation (7, 50). In fact, mRNAs vary widely in their inherent “translatability”, so they are preferentially and disproportionately affected when global translation is inhibited. For example, mTOR inhibitor, Torin 1, caused a severe defect in global protein synthesis, but a subset of mRNAs, so called top or top-like mRNAs, are specifically regulated by mTOR inhibition (50). Also, another subset of mRNAs which have lengthy, high G+C, highly structured 5’-UTRs, so called “weak” mRNAs, are particularly sensitive to alterations in eIF4E levels and eIF4F complex formation (7). In our study, depletion of eIF3b leads to decreased global translation, and more profoundly to a subset of mRNAs including cyclins and integrin α5. Interestingly, depletion of eIF3c induced similar changes on targeted proteins and cell morphology, suggesting that the eIF3 complex is disrupted by depletion of either eIF3 subunit. Comparative studies using polysome RNA microarray or other techniques will be needed to demonstrate if any RNAs are regulated in a subunit specific way.

In summary, our results indicate that eIF3b expression is necessary for multiple cellular processes including cell cycle progression, focal adhesion maintenance, tumorigenesis and progression in human cancer cells through global changes in translation and potentially through alteration in the rates of synthesis of specific proteins. Since we did not see depression of all proteins when depleting eIF3b levels in human cancer cells, we speculate that like eIF4E (7), eIF3b, might be another tractable pharmaceutical target for cancer treatment.

Supplementary Material

Refer to Web version on PubMed Central for supplementary material.

Acknowledgments

This work is supported by National Institutes of Health grants CA075115 and CA104106 to DT. JSK is an Early Career Scientist of the Howard Hughes Medical Institute.

REFERENCES

1. Silvera D, Formenti SC, Schneider RJ. Translational control in cancer. Nat Rev Cancer. 2010; 10:254–266. [PubMed: 20332778]

2. Pestova TV, Kolupaeva VG. The roles of individual eukaryotic translation initiation factors in ribosomal scanning and initiation codon selection. Genes Dev. 2002; 16:2906–2922. [PubMed: 12435632]
3. Sonenberg N, Hinnebusch AG. Regulation of translation initiation in eukaryotes: mechanisms and biological targets. Cell. 2009; 136:731–745. [PubMed: 19239892]
4. Hagner PR, Schneider A, Gartenhaus RB. Targeting the translational machinery as a novel treatment strategy for hematologic malignancies. Blood. 2010; 115:2127–2135. [PubMed: 20075156]
5. De Benedetti A, Graff JR. eIF-4E expression and its role in malignancies and metastases. Oncogene. 2004; 23:3189–3199. [PubMed: 15094768]
6. Graff JR, Konicek BW, Vincent TM, Lynch RL, Monteith D, Weir SN, et al. Therapeutic suppression of translation initiation factor eIF4E expression reduces tumor growth without toxicity. J Clin Invest. 2007; 117:2638–2648. [PubMed: 17786246]
7. Graff JR, Konicek BW, Carter JH, Marcusson EG. Targeting the eukaryotic translation initiation factor 4E for cancer therapy. Cancer Res. 2008; 68:631–634. [PubMed: 18245460]
8. Hsieh AC, Ruggero D. Targeting eukaryotic translation initiation factor 4E (eIF4E) in cancer. Clin Cancer Res. 2010; 16:4914–4920. [PubMed: 20702611]
9. Smith SC, Baras AS, Dancik G, Ru Y, Ding KF, Moskaluk CA, et al. A 20-gene model for molecular nodal staging of bladder cancer: development and prospective assessment. Lancet Oncol. 2011; 12:137–143. [PubMed: 21256081]
10. Smith SC, Baras AS, Owens CR, Dancik G, Theodorescu D. Transcriptional signatures of Ral GTPase are associated with aggressive clinicopathologic characteristics in human cancer. Cancer Res. 2012; 72:3480–3491. [PubMed: 22586063]
11. Dancik GM, Ru Y, Owens CR, Theodorescu D. A framework to select clinically relevant cancer cell lines for investigation by establishing their molecular similarity with primary human cancers. Cancer Res. 2011; 71:7398–7409. [PubMed: 22012889]
12. Hinnebusch AG. eIF3: a versatile scaffold for translation initiation complexes. Trends Biochem Sci. 2006; 31:553–562. [PubMed: 16920360]
13. Dong Z, Zhang JT. Initiation factor eIF3 and regulation of mRNA translation, cell growth, and cancer. Crit Rev Oncol Hematol. 2006; 59:169–180. [PubMed: 16829125]
14. Dong Z, Liu LH, Han B, Pincheira R, Zhang JT. Role of eIF3 p170 in controlling synthesis of ribonucleotide reductase M2 and cell growth. Oncogene. 2004; 23:3790–3801. [PubMed: 15094776]
15. Mayeur GL, Hershey JW. Malignant transformation by the eukaryotic translation initiation factor 3 subunit p48 (eIF3e). FEBS Lett. 2002; 514:49–54. [PubMed: 11904180]
16. Cappuzzo F, Varella-Garcia M, Rossi E, Gajapathy S, Valente M, Drabkin H, et al. MYC and EIF3H Coamplification significantly improve response and survival of non-small cell lung cancer patients (NSCLC) treated with gefitinib. J Thorac Oncol. 2009; 4:472–478. [PubMed: 19204574]
17. Saramaki O, Willi N, Bratt O, Gasser TC, Koivisto P, Nupponen NN, et al. Amplification of EIF3S3 gene is associated with advanced stage in prostate cancer. Am J Pathol. 2001; 159:2089–2094. [PubMed: 11733359]
18. Zhou M, Sandercock AM, Fraser CS, Ridlova G, Stephens E, Schenauer MR, et al. Mass spectrometry reveals modularity and a complete subunit interaction map of the eukaryotic translation factor eIF3. Proc Natl Acad Sci U S A. 2008; 105:18139–18144. [PubMed: 18599441]
19. Herrmannova A, Daujotyte D, Yang JC, Cuchalova L, Gorrec F, Wagner S, et al. Structural analysis of an eIF3 subcomplex reveals conserved interactions required for a stable and proper translation pre-initiation complex assembly. Nucleic Acids Res. 2012; 40:2294–2311. [PubMed: 22090426]
20. Zhang L, Pan X, Hershey JW. Individual overexpression of five subunits of human translation initiation factor eIF3 promotes malignant transformation of immortal fibroblast cells. J Biol Chem. 2007; 282:5790–5800. [PubMed: 17170115]
21. Lin L, Holbro T, Alonso G, Gerosa D, Burger MM. Molecular interaction between human tumor marker protein p150, the largest subunit of eIF3, and intermediate filament protein K7. J Cell Biochem. 2001; 80:483–490. [PubMed: 11169732]

22. Kim WJ, Kim EJ, Kim SK, Kim YJ, Ha YS, Jeong P, et al. Predictive value of progression-related gene classifier in primary non-muscle invasive bladder cancer. Mol Cancer. 2010; 9:3. [PubMed: 20059769]
23. Stransky N, Vallot C, Reyal F, Bernard-Pierrot I, de Medina SG, Segraves R, et al. Regional copy number-independent deregulation of transcription in cancer. Nat Genet. 2006; 38:1386–1396. [PubMed: 17099711]
24. Irizarry RA, Hobbs B, Collin F, Beazer-Barclay YD, Antonellis KJ, Scherf U, et al. Exploration, normalization, and summaries of high density oligonucleotide array probe level data. Biostatistics. 2003; 4:249–264. [PubMed: 12925520]
25. Said N, Smith S, Sanchez-Carbayo M, Theodorescu D. Tumor endothelin-1 enhances metastatic colonization of the lung in mouse xenograft models of bladder cancer. J Clin Invest. 2011; 121:132–147. [PubMed: 21183790]
26. Nicholson BE, Frierson HF, Conaway MR, Seraj JM, Harding MA, Hampton GM, et al. Profiling the evolution of human metastatic bladder cancer. Cancer Res. 2004; 64:7813–7821. [PubMed: 15520187]
27. Smith SC, Oxford G, Wu Z, Nitz MD, Conaway M, Frierson HF, et al. The metastasis-associated gene CD24 is regulated by Ral GTPase and is a mediator of cell proliferation and survival in human cancer. Cancer Res. 2006; 66:1917–1922. [PubMed: 16488989]
28. Oxford G, Owens CR, Titus BJ, Foreman TL, Herlevsen MC, Smith SC, et al. RalA and RalB: antagonistic relatives in cancer cell migration. Cancer Res. 2005; 65:7111–7120. [PubMed: 16103060]
29. Gildea JJ, Golden WL, Harding MA, Theodorescu D. Genetic and phenotypic changes associated with the acquisition of tumorigenicity in human bladder cancer. Genes Chromosomes Cancer. 2000; 27:252–263. [PubMed: 10679914]
30. Wu Y, McRoberts K, Berr SS, Frierson HF Jr, Conaway M, Theodorescu D. Neuromedin U is regulated by the metastasis suppressor RhoGDI2 and is a novel promoter of tumor formation, lung metastasis and cancer cachexia. Oncogene. 2007; 26:765–773. [PubMed: 16878152]
31. Gildea JJ, Seraj MJ, Oxford G, Harding MA, Hampton GM, Moskaluk CA, et al. RhoGDI2 is an invasion and metastasis suppressor gene in human cancer. Cancer Res. 2002; 62:6418–6423. [PubMed: 12438227]
32. Dransart E, Olofsson B, Cherfils J. RhoGDIs revisited: novel roles in Rho regulation. Traffic. 2005; 6:957–966. [PubMed: 16190977]
33. Harding MA, Theodorescu D. RhoGDI signaling provides targets for cancer therapy. Eur J Cancer. 2010; 46:1252–1259. [PubMed: 20347589]
34. Parsons JT, Horwitz AR, Schwartz MA. Cell adhesion: integrating cytoskeletal dynamics and cellular tension. Nat Rev Mol Cell Biol. 2010; 11:633–643. [PubMed: 20729930]
35. Duxbury MS, Ito H, Zinner MJ, Ashley SW, Whang EE. Focal adhesion kinase gene silencing promotes anoikis and suppresses metastasis of human pancreatic adenocarcinoma cells. Surgery. 2004; 135:555–562. [PubMed: 15118593]
36. Sakamoto S, McCann RO, Dhir R, Kyprianou N. Talin1 promotes tumor invasion and metastasis via focal adhesion signaling and anoikis resistance. Cancer Res. 2010; 70:1885–1895. [PubMed: 20160039]
37. Parsons JT. Focal adhesion kinase: the first ten years. J Cell Sci. 2003; 116:1409–1416. [PubMed: 12640026]
38. Mitra SK, Hanson DA, Schlaepfer DD. Focal adhesion kinase: in command and control of cell motility. Nat Rev Mol Cell Biol. 2005; 6:56–68. [PubMed: 15688067]
39. Rothe M, Ko Y, Albers P, Wernert N. Eukaryotic initiation factor 3 p110 mRNA is overexpressed in testicular seminomas. Am J Pathol. 2000; 157:1597–1604. [PubMed: 11073819]
40. Overdevest JB, Thomas S, Kristiansen G, Hansel DE, Smith SC, Theodorescu D. CD24 offers a therapeutic target for control of bladder cancer metastasis based on a requirement for lung colonization. Cancer Res. 2011; 71:3802–3811. [PubMed: 21482678]
41. Giacinti C, Giordano A. RB and cell cycle progression. Oncogene. 2006; 25:5220–5227. [PubMed: 16936740]

42. Jorgensen P, Tyers M. How cells coordinate growth and division. Curr Biol. 2004; 14:R1014–R1027. [PubMed: 15589139]
43. Liang H, Ding X, Zhou C, Zhang Y, Xu M, Zhang C, et al. Knockdown of eukaryotic translation initiation factors 3B (EIF3B) inhibits proliferation and promotes apoptosis in glioblastoma cells. Neurol Sci. 2012
44. Wang Z, Chen J, Sun J, Cui Z, Wu H. RNA Interference-Mediated Silencing of Eukaryotic Translation Initiation Factor 3, Subunit B (EIF3B) Gene Expression Inhibits Proliferation of Colon Cancer Cells. World J Surg Oncol. 2012; 10:119. [PubMed: 22734884]
45. Ridley AJ, Schwartz MA, Burridge K, Firtel RA, Ginsberg MH, Borisy G, et al. Cell migration: integrating signals from front to back. Science. 2003; 302:1704–1709. [PubMed: 14657486]
46. Schwartz MA. Integrin signaling revisited. Trends Cell Biol. 2001; 11:466–470. [PubMed: 11719050]
47. Morozevich G, Kozlova N, Cheglakov I, Ushakova N, Berman A. Integrin alpha5beta1 controls invasion of human breast carcinoma cells by direct and indirect modulation of MMP-2 collagenase activity. Cell Cycle. 2009; 8:2219–2225. [PubMed: 19617714]
48. Mierke CT, Frey B, Fellner M, Herrmann M, Fabry B. Integrin alpha5beta1 facilitates cancer cell invasion through enhanced contractile forces. J Cell Sci. 2011; 124:369–383. [PubMed: 21224397]
49. Sawada K, Mitra AK, Radjabi AR, Bhaskar V, Kistner EO, Tretiakova M, et al. Loss of E-cadherin promotes ovarian cancer metastasis via alpha 5-integrin, which is a therapeutic target. Cancer Res. 2008; 68:2329–2339. [PubMed: 18381440]
50. Thoreen CC, Chantranupong L, Keys HR, Wang T, Gray NS, Sabatini DM. A unifying model for mTORC1-mediated regulation of mRNA translation. Nature. 2012; 485:109–113. [PubMed: 22552098]

TRANSLATIONAL RELEVANCE

Cap-dependent pathway of translation initiation in eukaryotes is promoted by eukaryotic initiation factor (eIFs) proteins. While several eIF proteins are overexpressed in cancer, few have been conclusively implicated as drivers of human cell transformation, cancer progression or patient outcome. Here we show for the first time that eukaryotic initiation factor 3b (eIF3b) expression is associated with stage, grade and outcome in patients with bladder and prostate cancer. In addition, using multiple complementary molecular and preclinical animal studies in models of bladder and prostate cancer, we demonstrate that eIF3b regulates primary tumor growth and lung colonization. Together, this data suggests that eIF3b may be a viable therapeutic target.

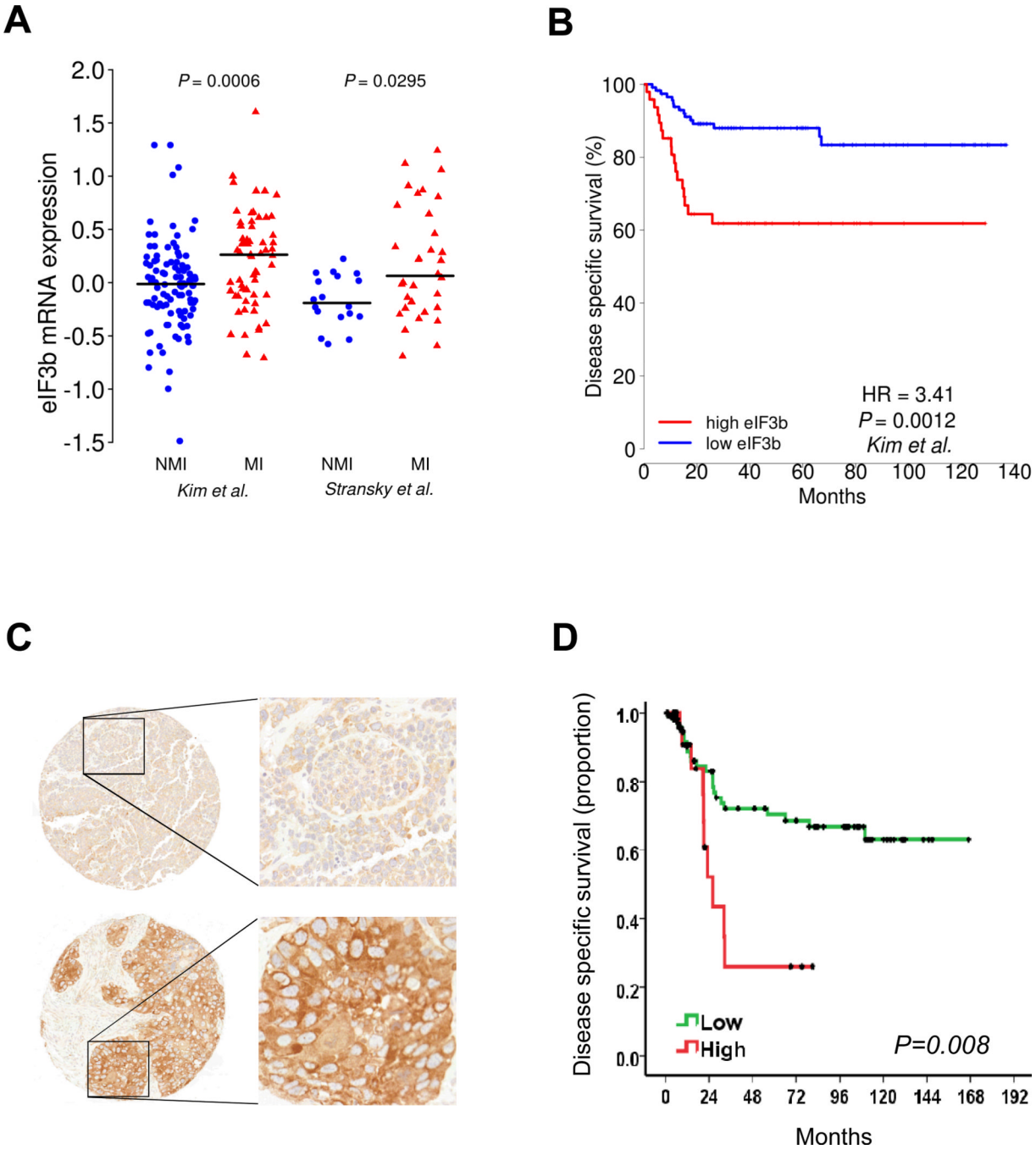

Figure 1. High expression of eIF3b is associated with aggressive phenotypes and poor outcome in bladder cancer patients

Higher mRNA expression of eIF3b is associated with (**A**) muscle invasive (MI, pT2 and above); versus non-muscle invasive (NMI, pTa and pT1)) samples and (**B**) worse disease specific survival. In **A**, eIF3b expression data are plotted and their median expression is specified by horizontal lines. P-values of the difference between the two groups were determined by the Mann-Whitney U test. In **D**, patients were divided into two groups based on percentile expression (high eIF3b ≥ 70^{th} percentile and low eIF3b < 70^{th} percentile) and compared using Cox proportional hazards models and log rank tests (see Materials and Methods). Hazard ratios and adjusted log rank P-values are shown. Higher protein

expression of eIF3b is associated with (**C**) muscle invasive (MI) versus non-muscle invasive (NMI) samples and (**D**) worse disease specific survival. **C**, Representative immunohistochemistry shows that the expression patterns of eIF3b in NMI (upper panel) and MI (lower panel) bladder tumors contained in tissue arrays. (Original magnifications: ×200 left panel, and ×400 right panel). **D**, Kaplan-Mayer curve plot shows stratification of disease specific survival for all patients as a function of tumor cytoplasmic eIF3b staining. High: tumors expressing cytoplasmic eIF3b in at least 80% of the cancer cells; Low: All other tumors (log rank, p-0.008).

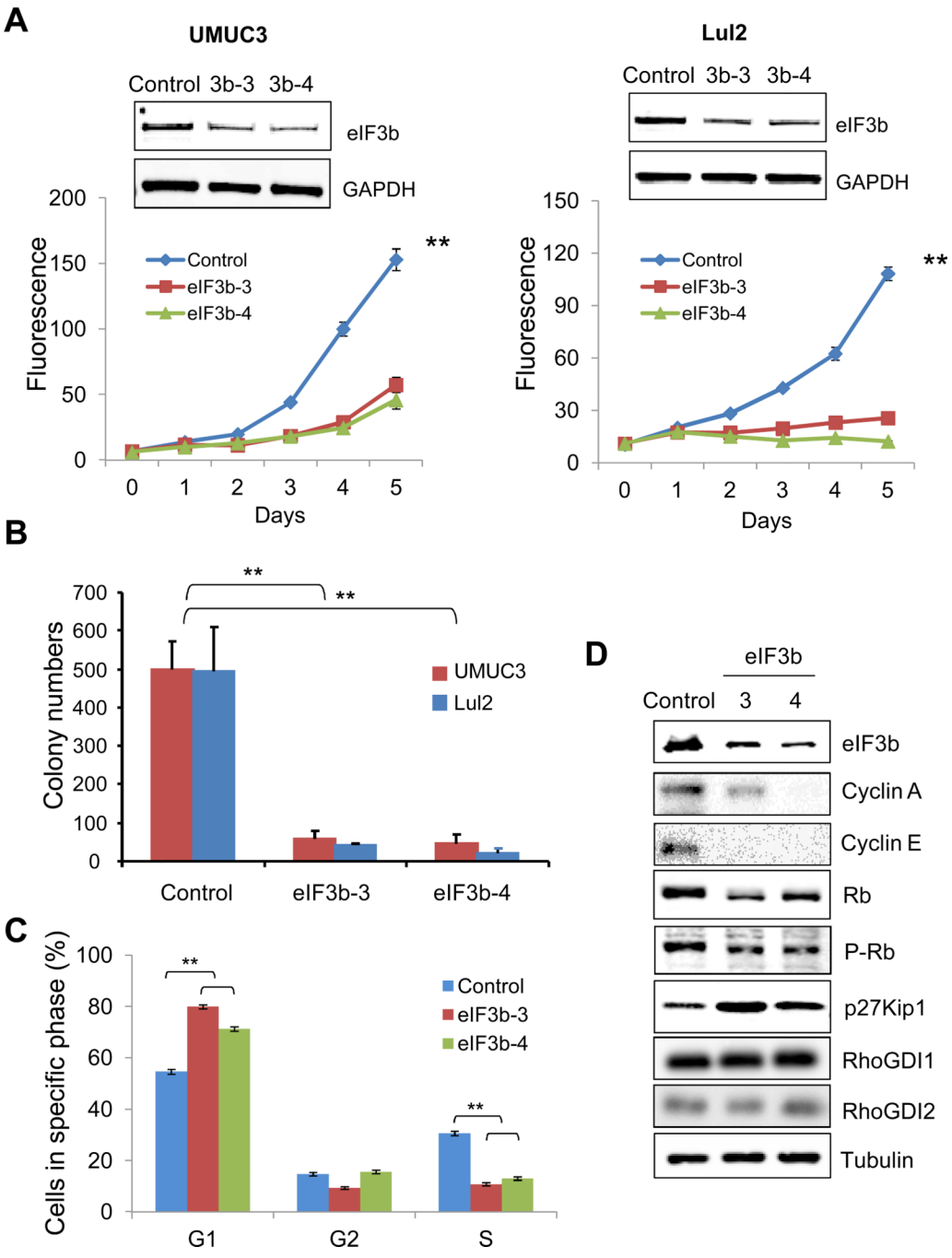

Figure 2. Depletion of eIF3b inhibits bladder cancer cell growth by inhibition of G1/S transition of the cell cycle

(**A**) eIF3b was depleted by eIF3b siRNAs (oligos eIF3b-3 and eIF3b-4) in UMUC3 and Lul2 human bladder cancer cells. Cell growth was evaluated over five days by the alamarBlue assay. Data shown is the mean ± S.D. of fluorescence intensity of triplicate wells in two separate experiments (**, $p<0.01$, by t-Test). Western blotting shows the reduced levels of eIF3b. GAPDH was used as a loading control. (**B**) Colony formation was measured by a soft agar assay in UMUC3 and Lul2 cells three weeks after transfection of eIF3b or control GL2 siRNA from above. Graph shows the mean ± S.D. of colony numbers of triplicate wells in three separate experiments (**, $p<0.01$, by t-Test). (**C**) Flow cytometry analysis was

performed in UMUC3 cells transfected with the indicated eIF3b or control GL2 siRNA. Graph shows the mean ± S.D. of percentage of cells in G1, G2 or S from two independent experiments (**, $p<0.01$, by t-Test). (**D**) The samples from flow cytometry were analyzed by Western blots with indicated antibodies. α-tubulin was used as a loading control.

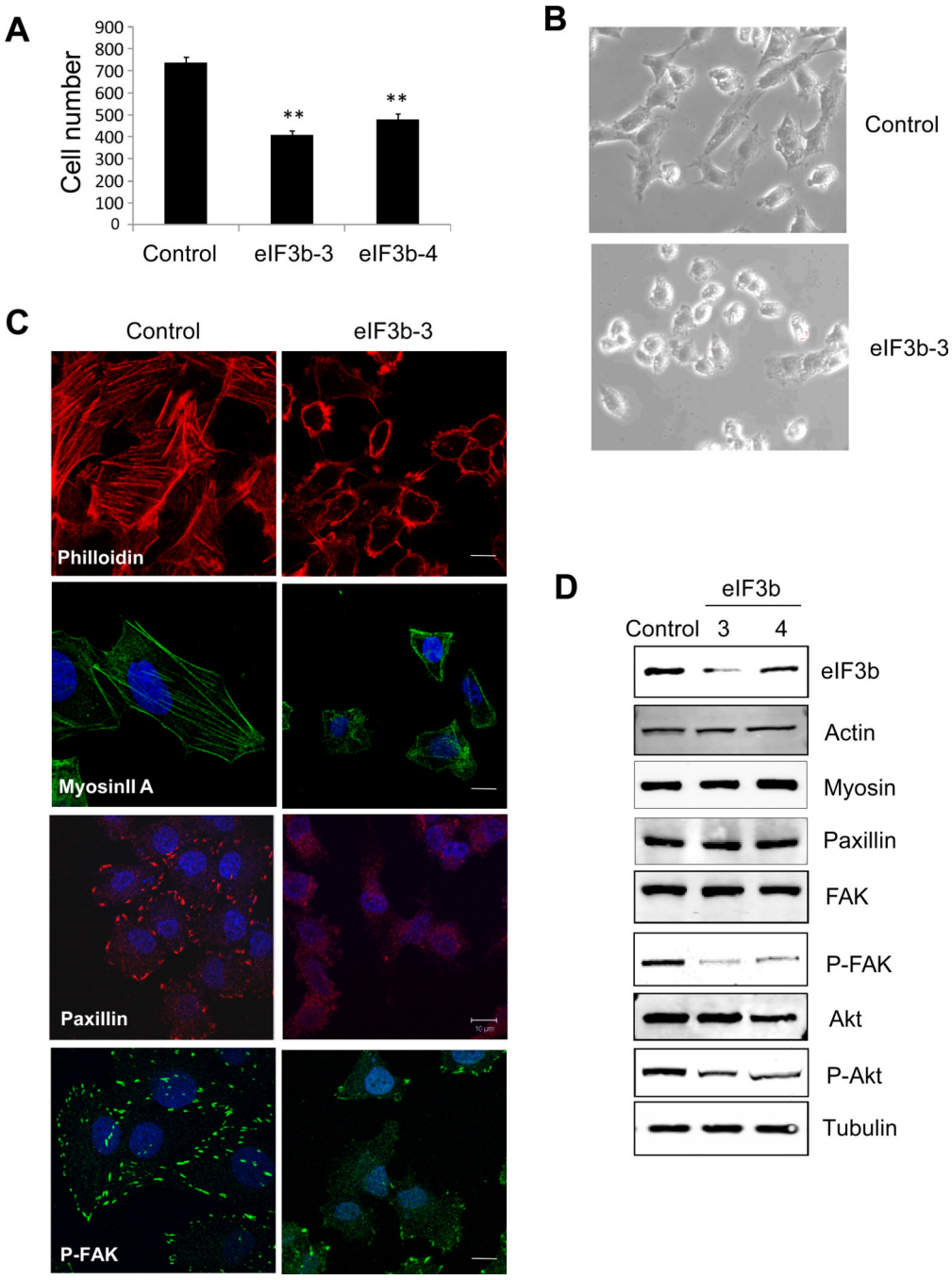

Figure 3. Depletion of eIF3b inhibits bladder cancer cell migration and disrupts actin cytoskeleton organization and focal adhesion

(**A**) Cell migration was measured by the Boyden chambers assay. UMUC3 cells transfected with eIF3b or control siRNA were seeded onto Boyden chambers after 72 hours. Cells that migrated through the chambers were counted after 5 hours. Data shown is the mean ± S.D. of migrated cells from triplicate experiments. (**, $p<0.01$, by t-Test). (**B**) Phase contrast images of UMUC3 cells transfected with control GL2 and eIF3b siRNA. (**C**) Confocal immunofluorescence images of UMUC3 cells transfected with control GL2 and eIF3b siRNA (phalloidin for actin, red; anti-myosin IIA, green; anti-Paxillin, red; anti-P-FAK, green and DAPI, blue; scale bar is 10 μm). (**D**) Replicates of cells used for the above images

were analyzed by Western blotting with indicated antibodies. α-tubulin was used as a loading control.

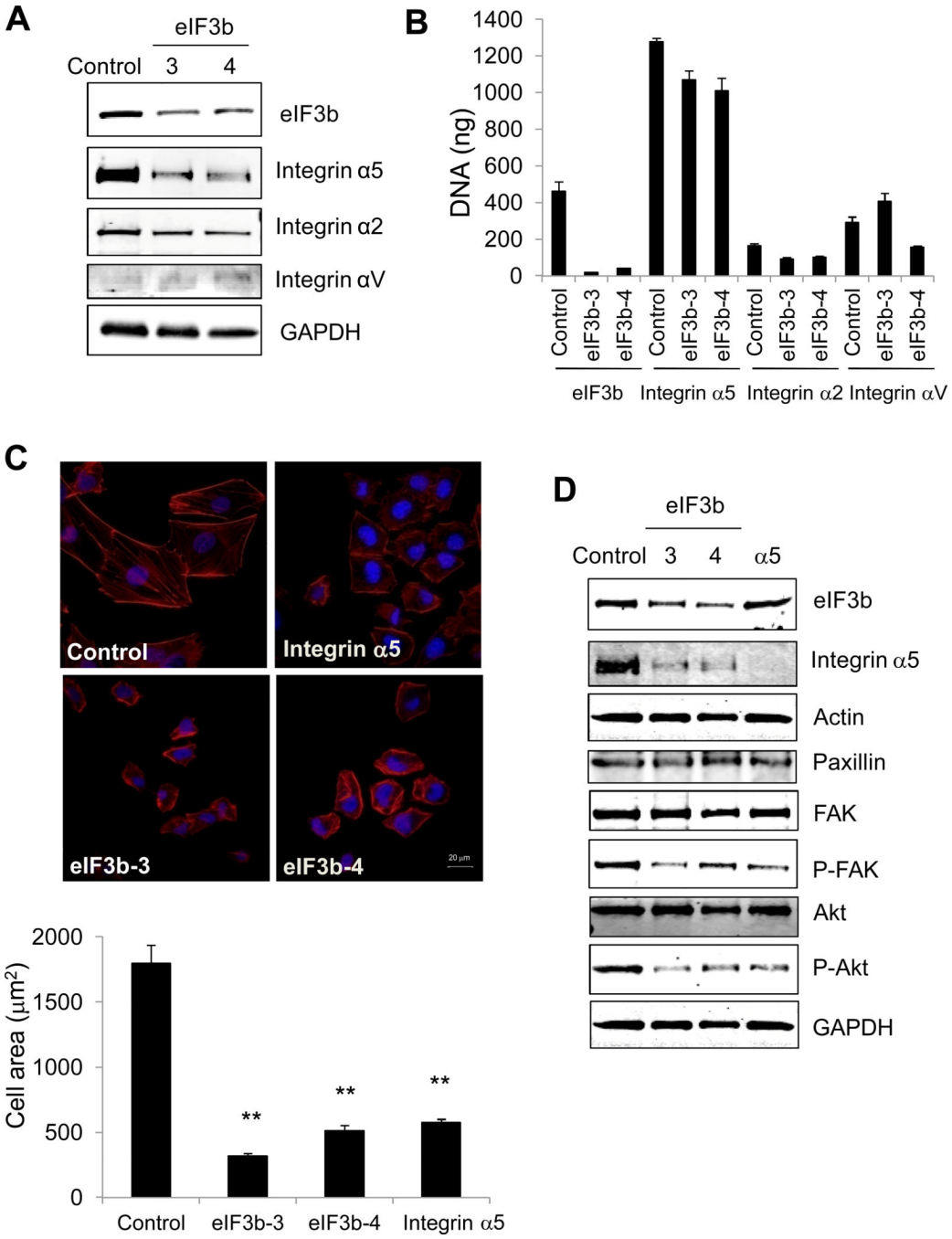

Figure 4. Depletion of eIF3b inhibits integrin α5 expression and depletion of integrin α5 interrupts actin cytoskeleton organization in UMUC3 cells

(**A**) Graph shows Western blot analysis of integrin protein expression in UMUC cells with eIF3b depletion. GAPDH was used as a loading control. (**B**) Real-time PCR indicates the mRNA level of eIF3b and integrin protein from eIF3b-depleted UMUC3 cells. Graph shows the mean ± S.D of DNA amount (ng), measured in triplicate in two independent experiments. (**C**) Confocal immunofluorescence images of UMUC3 cells transfected with control GL2, eIF3b or integrin α5 siRNA (phalloidin for actin, red; DAPI, blue; scale bar is 20 μm) (upper panel). The areas of the cells from the above images were quantified using ImageJ. The result is shown as the mean ± S.D of average area of cells (μm^2) (lower panel)

(**, $p<0.01$, by t-Test). (**D**) Replicates of cells used for the above images were analyzed by Western blotting with indicated antibodies. GAPDH was used as loading control.

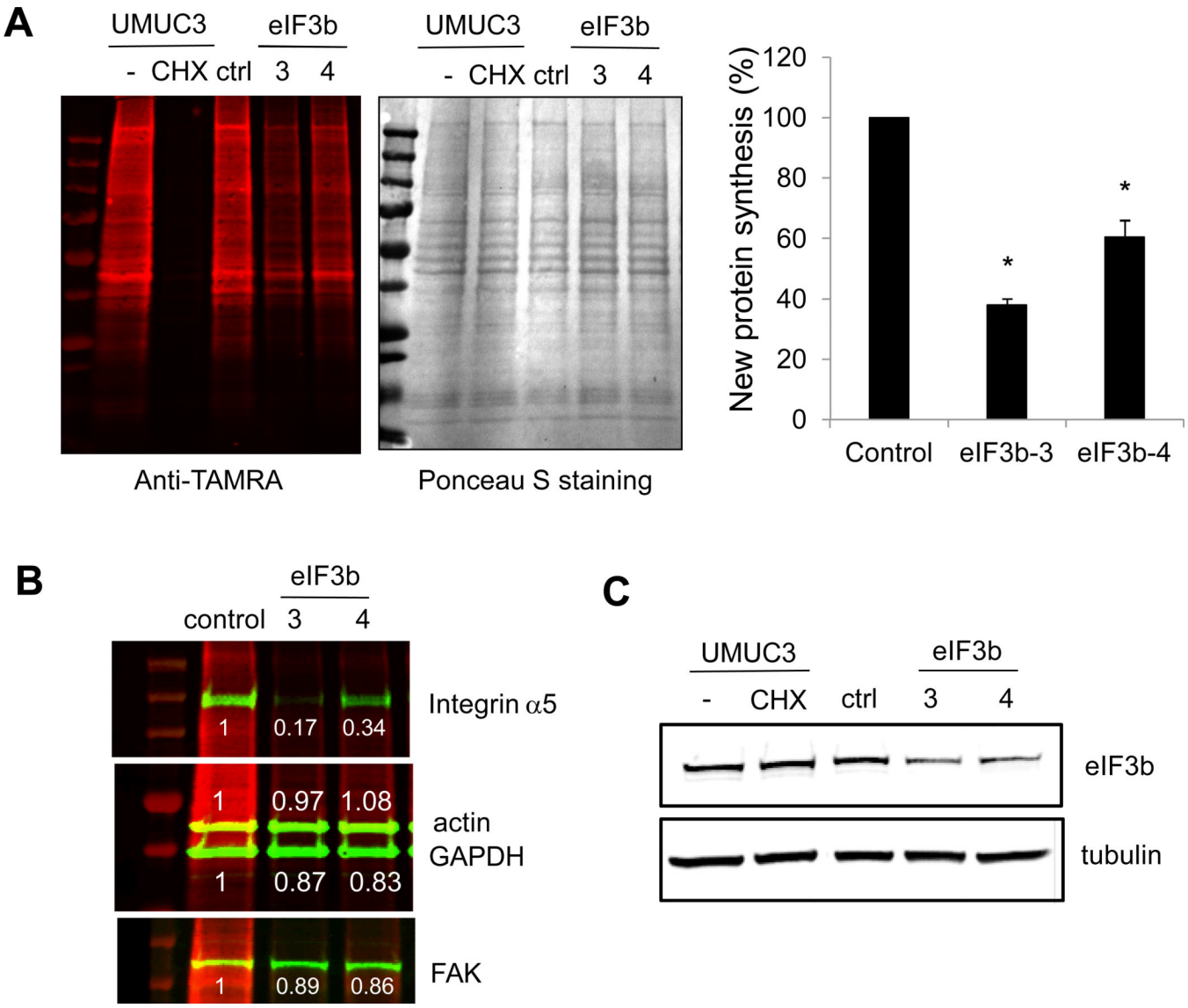

Figure 5. eIF3b knockdown inhibits new protein synthesis

(**A**) UMUC3 cells transfected with eIF3b siRNA or control siRNA were labeled with AHA for 2 hours. Newly synthesized proteins was detected by Click-iT assay using an anti-TAMRA antibody. Untreated UMUC3 cells were used as a positive control and cycloheximide (CHX) treatment was a control for total protein synthesis reduction. Ponceau S staining for total protein served as a loading control. Protein ladder is shown in the first lane. The graph shows the relative amount of newly synthesized protein as the mean ± S.D. from two experiments (* $p<0.05$). (**B**) The total proteins in each reaction were detected by indicated antibodies. Quantification of band intensity relative to control siRNA is shown. (**C**) eIF3b protein levels were checked by anti-eIF3b antibody and anti-α-tubulin was used as loading control.

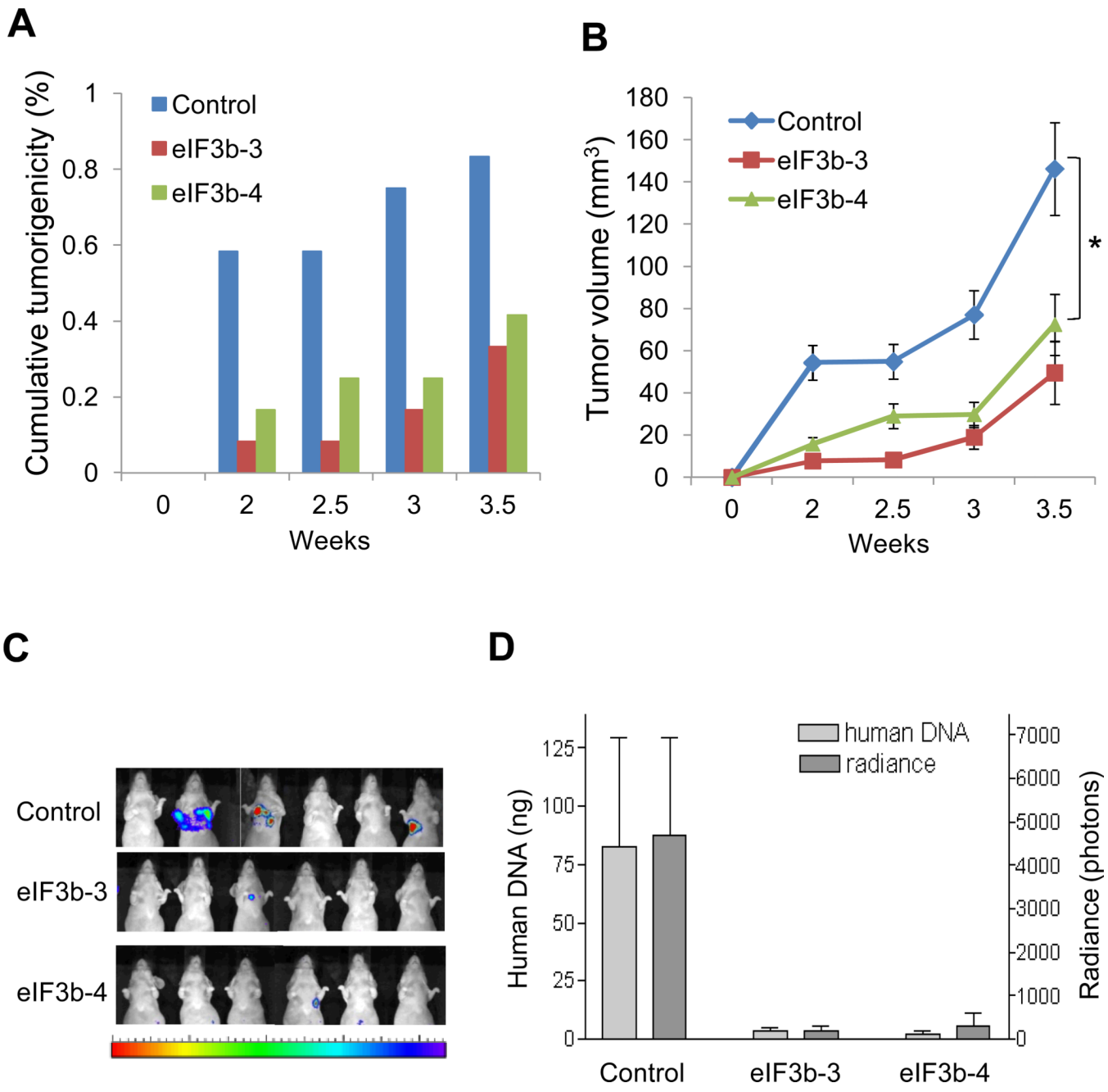

Figure 6. eIF3b knockdown inhibits subcutaneous tumor growth and lung colonization in bladder tumor cells

(**A–B**), UMUC3 cells transfected with eIF3b siRNA (eIF3b-3, eIF3b-4) or control GL2 siRNA were injected into mice subcutaneously 24 hours after transfection (n=5 for each group). (**A**) Measurable tumor formation over the time of each group (%) is shown. (**B**) The average tumor volume of each is shown as the mean ± S.D of tumor volume (mm^3). Graph shown is the growth of only tumors that took (*, p=0.034). (**C–D**), Lul2 cells transfected with eIF3b siRNA or control GL2 siRNA were injected into mice via tail vein 24 hours after transfection (n=10 for each group). (**C**) Representative bioluminescent images at 5 weeks after injection are shown. (**D**) The radiance of luciferase signals from the images was quantified using Living Image 2.60 software. The result is shown as the mean ± S.D of

radiance (photons) (right Y Axis). Quantitation of human tumor DNA in the mouse lungs at 5 weeks after injection was done by real time PCR using specific human 12p primers. Result is shown as the mean ± S.D. of human DNA amount (ng) in 500 ng of mouse lung DNA of each group of mice from triplicate PCR reactions (left Y Axis).